Received: 19 September 2023 | Revised: 27 November 2023 | Accepted: 4 December 2023

DOI: 10.1002/ese3.1649

ORIGINAL ARTICLE

Numerical and experimental investigation of an Archimedes screw turbine for open channel water flow application

Zeshan Abbas[1] | **Muhammad Waqas**[2] | **Saad Saleem Khan**[3] | **Rabia Khatoon**[4] | **Stephen Larkin**[5] | **Lun Zhao**[1]

[1]Institute of Ultrasonic Technology, Shenzhen Polytechnic University, Shenzhen, China

[2]Mechanical Engineering Department, Pakistan Institute of Engineering and Technology, Multan, Pakistan

[3]United Arab Emirates University, Al-Ain, UAE

[4]London Centre for Energy Engineering School of Engineering, London South Bank University, London, UK

[5]Africa New Energies Ltd., London, UK

Correspondence
Lun Zhao, Institute of Ultrasonic Technology, Shenzhen Polytechnic University, Shenzhen 518055, China.
Email: zhaolun@szpu.edu.cn

Funding information
Africa New Energies Limited, UK and National Natural Science Foundation of China, Grant/Award Number: 12104324; Scientific Research Startup Fund for Shenzhen High-Caliber Personnel of SZPT, Grant/Award Number: 6022310046K; Postdoctoral Startup Fund of Shenzhen Polytechnic University, Grant/Award Numbers: 6021330001K, 6022331008K

Abstract

Low-head turbines are becoming an agricultural imperative due to their high efficiency, low cost, ability to operate at low flow rates and minimal environmental impact. Therefore, the Archimedes screw turbine (AST) can play a leading role for producing electric power, especially in Pakistan's rural areas where most of the places have less than 1 m head. In this research work, performance evaluation of AST was carried out at different flow velocities in terms of power coefficient and torque generated. Design parameters such as blade width, blade pitches, and blade rotational angles are also used for performance evaluation. For this purpose, computational fluid dynamic (CFD) analyses of AST blades were conducted at different water flow velocities (e.g., 1, 1.5, 2, 2.5, 3, and 3.5 m/s). ANSYS FLUENT was used for AST blade simulations using three different design parameters such as blade width, blade pitch, and blade rotational angles. Additionally, CFD simulations have inherent errors and uncertainties that may lead to findings and deviations from their exact or real values. To prevent these uncertainties and errors, an experimental study was also conducted to provide validation for the CFD simulation results. The results revealed from CFD simulations for optimized design parameters were then compared with experimental data. From the results, it was examined that the numerical findings were in good agreement with the experiment data. The highest power coefficient and power output values were obtained under optimized design parameters such as inner and outer diameter, blade pitch, blade width, blade rotation angles and shaft length (e.g., 40 mm, 120 mm, 130 mm, 2 mm, 60°, and 850 mm respectively). The findings can be useful to implement the AST unit for those places where the available water head is ranging from 1 to 6.5 m and a flow rate of 0.2–6.5 m^3/s, especially for rural areas of Pakistan.

KEYWORDS
ANSYS FLUENT, Archimedes screw turbine, blade rotational angles, blade width and pitch, computational fluid dynamic

1 | INTRODUCTION

Nowadays, developing countries are facing multiple challenges to meet the energy demand and supply gap around the world. It has also been studied that numerous developing countries are facing energy and environmental issues. Carbon emissions have dangerous impacts on the environment. Renewable energy sources are the best solution to mitigate emissions and meet energy demands compared to other energy sources. Also, renewable energy is one of the most prominent energy sources to fill the energy demand and supply gap. Among all renewable energy sources, hydropower is the most widely used energy source as it is a clean, safe and emission-free source of energy. The developments of micro-hydropower plants, especially low head turbines have attracted more attention in recent years. Similarly, about 22.8% of global power generation pertains to hydro, wind, solar, and geothermal energy.[1] The extraction of energy from water is also considered a useful sustainable energy resource since it is a clean and emission-less source of energy. However, the development of hydro power in recent years represents that total hydropower will increase to 1400 GW by 2035.[2] In addition, large dam sites require a lot of money and take about 5 or 6 years to complete. So, many different ideas have been developed such as energy harvesting from small rivers, canals, and other irrigation streamlines and waste water systems.[3] Therefore, the extraction of kinetic energy from flowing water is new horizons for the use of water. Similarly, instead of the potential source of gravitational energy, a sustainable energy resource with a lower environmental impact may be produced.[4]

Archimedes screw turbine (AST) is an emergent form of micro-hydroelectric power generation system which is widely used to generate hydroelectric power in those areas where the available water is ranging from 1 to 6.5 m and a flow rate of 0.2–6.5 m^3/s.[5] The main component of an AST is the Archimedes screw. An Archimedes screw is made up of a series of interlaced helicoid planes connected to a central cylindrical shaft. The screw is contained within a trough that surrounds it. The screw may usually spin freely inside the fixed trough since there is a tiny space between the two. However, on rare occasions the crib is directly attached to the screw flights and rotates together with them. Water enters the top (inlet) of an inclined AST and travels through the screw from high elevation to low elevation. Then, it leaves at the end of the screw (outlet). The water traveling along the axial length of the screw is trapped between two successive screw flights, which generate discrete volume units known as buckets. The different water levels on either side of the screw flights are caused by the slanted orientation of the individual buckets relative to the screw axis, which creates a net pressure difference across the flights. Part of this pressure force acts tangentially to the central axis of the screw due to the helical structure of the flights. It further produces a torque that causes the screw to mechanically rotate. This mechanical revolution can produce power if a generator is fastened to the screw. Computational fluid dynamics (CFD) is an important tool that is widely used to examine the flow characteristics and performance of hydro turbines. By using CFD, gap flows, overflow flows and internal bucket flow patterns can all be analyzed which can isolate factors and provide a significant amount of information.[6]

Zitti et al.[7] investigated the efficiency of hydro Archimedes turbine using experimental approaches for low tip speed ratio (TSR) regimes. In addition, they also conducted a numerical simulation to assess the performance of hydro turbines. They also studied the performance curve of turbines in both aligned and inclined configurations. Shahverdi et al.[8] developed an energy harvesting model to generate electrical power by combining the AST turbine and solar organic Rankine cycle (ORC) system. An AST using a numerical approach for mechanical power generation as an energy harvesting technique is investigated. They took into account variables such as screw inclination angle, number of flights, and screw length. Monatrakul et al.[9] presented that the spiral hydro turbine's horizontal axis's spiral blade angle has a substantial impact on its performance. To ensure the turbine performs to its full potential in this study, CFD analysis was also carried out. Li et al.[10] conducted a CFD analysis on the reversible pump turbine impeller to look into the impact of hydraulic force. It has been shown that the guide vane apertures and operation circumstances have an impact on the force's amplitude and prominent components. Bouvant et al.[11] evaluated the performance of AST in terms of coefficient of power. The study examined the performance of AST with different variables such as inner and outer diameter, blade inclination angle, and axle length. They considered CFD simulations to examine the interaction among the referred parameters on the turbine performance. Shahverdi et al.[12] developed a numerical model to examine the performance of AST for replacing in irrigation canals instead of current check structures. They also validated and developed numerical models with experimental results and found satisfactory evaluations. Riglin et al.[13] developed a model with a variety of optimization and characterization analyses at various flow rates. Also, it was discovered that while manually loading, the largest coefficient of power is 0.37 at a TSR of 2.5 m/s. Moreover, the relative error of 3.0% was projected between the numerical and experimental

findings. Yang et al.[14] investigated the impact of blade thickness to examine the effectiveness of the pump as a turbine (PAT). Likewise, it looked into how turbine performance varies with blade thickness. Dedi et al.[15] investigated and designed a small-scale AST using an experimental approach. The study also conducted performance analysis with different parameters such as water flow ratio, inclination angles and rotation speed using experimentally with respect to turbine power output, torque, and efficiency. Dellinger et al.[16] performed a CFD analyses of AST and experimental analyses to examine the performance of AST turbines at different variables such as inclination angles and number of blades. It found good agreement between numerical and experimental results. Daskiran et al.[17] carried out a CFD investigation on a vented micro propeller turbine operating in both design and off-design conditions. Similarly, it is observed that tiny propeller turbines may be employed effectively for aeration under various operating circumstances. Riglin et al.[18] examined the two diffuser designs with value area ratios of 1.36 and 2.01 based on CFD research. Moreover, a 55.8% increase in output mechanical power was noted. Teran et al.[19] carried out a CFD study to create a new geometry with higher efficiency. The projected efficiency of the revised geometry created by the CFD study was 14.77%. Erinofiardi et al.[20] carried out performance analysis of screw turbine using the experimental approach. It was examined that the screw turbine can generate 1.4 W of maximum power with 49% efficiency at a 22° angle of inclination with an outer diameter of 142 mm and water flow rate of 1.2 l/sec with a head of 0.25 m. Kozyn et al.[21] presented a complete model of power loss for an AST which was used for power generation including a nondimensional model to predict power losses due to outlet submersion flooding. Lee et al.[22] started a study with a conceptual design based on literature review findings. The STUDY built and tested the AST in the experimental laboratory to examine the performance of turbines. Lisick et al.[23] presented the approach for the community by effectively maximizing the AST's design and operation for a given installation's overall rate of return. Liu et al.[24] proposed a workable regional integrated energy system that maintained high use of photo thermal resources while generating steam from CHP to fulfill both electric and heat demands. They also created a model of a 600 MW CHP with a screw turbine and pressure matcher in Ebsilon Software. Piper et al.[25] suggested acoustic and passive integrated transponder telemetry, as well as dual frequency image sonar, to investigate the impact of an AST and accompanying fish passes on the movement patterns and behavior of five species of potadromous fish. Rohmer et al.[26] discussed an optimal sizing of AST based on a previous study. Then, they proposed a numerical model to determine the mechanical efficiency based on its geometrical configuration and its rotational speed. Siswantara et al.[27] examined the impact of alpha angle on the performance of the AST using an experimental approach. They performed the experimental analyses with discharge of 0.00106 m^3/s and the angles between ranging of 36° and 44° and three different loads. The study also examined the causes of overflow that was lost at different angles. Kamal et al.[28] explored the efficient conversion of traditional water mill into micro hydropower system in western Himalayan region of India. They conducted experimental study to design and investigation of performance of micro hydropower system. They examined from the revealed outcomes that the screw angle ranges 20°–25° and flow rate less than 1.5 L/s enhanced the efficiency of hydropower system up to 90% using Archimedes Screw mechanism. Adeel et al.[29] presented the study using CFD analysis on 3D numerical simulation of water flow stable turbulent in the passage of an AST. They performed numerical simulations with different number of turbine blades using ANSYS FLUENT. Kamal et al.[30] conducted a comprehensive feasibility analysis for conversion of existing traditional watermills in Western Himalayan region of India to micro-hydropower plants using a low head AST for rural electrification. They investigated that it is quite feasible and economical to use existing watermills for power generation using AST. Neeraj et al.[31] conducted experimental study to examine the performance of AST at different input parameters. The experimental study revealed that the maximum efficiency of 74.27% is observed at 22° with flow rate of 1 L/s and load of 0.9 kg. They also examined that the maximum power output at given parameters is 0.00577 kW at load of 0.9 kg and flow rate of 4 L/s and tilt angle of 25°. Finally, it is concluded from the study that it is feasible to install AST at low head sites with low tilt angle and heavy load. Man et al.[22] conducted a performance analysis using experimental approaches with different operating parameters. Primarily, the study finalized the conceptual design based on existing literature review and then created a prototype of the laboratory setup. Afterwards, they carried out experiments at different parameters such as inclination angle and water flow velocities. The results revealed the optimum outcomes at an inclination angle of 45° with water flow velocity of 1–1.5 m/s. According to the aforementioned literature, most of the studies are presented related to hydropower, which has focused on energy conversion in the presence of high head and larger flow rates. Since most of the turbine systems have been fabricated on a large scale. There is limited studies

were found related to micro-hydro turbine systems which produce power in the low head and free stream flow condition. In addition, it has been studied from the current literature that most of the authors have worked on some aspects of geometric parameters such as number of blades and inclination angles, and so forth. A study of all process parameters and geometric matrices has not yet been performed e.g., flow velocities, blade width, blade rotational angles, and blade pitch to examine the performance of the AST.

In this research work, designing, prototyping, and performance evaluation of AST turbine with different flow and geometric parameters such as flow velocity, blade width, blade rotation angles, and blade pitch are investigated. For this purpose, CFD simulations were performed at different flow velocities and different geometrical parameters such as blade pitch, blade width, and blade rotational angles to observe the flow characteristics such as pressure distribution, velocity distribution, and flow rates. The ANSYS FLUENT was used for the CFD simulations. CFD simulations allow the control and precise determination of parameters that cannot be directly observed in the experimental approach. Therefore, in CFD simulations, the influence of changing flow and geometric parameters can be clearly observed. To reduce some uncertainties and errors in the exact or real values, an experimental study was also conducted to provide validation for the CFD simulation results.

2 | DESIGN CONSIDERATION AND PERFORMANCE PARAMETERS

The solid design consideration plays an essential role in the performance evaluation of AST. Therefore, an appropriate design scheme and description of performance parameters are necessary to execute. Most of the cases, AST only possess potential energy of the fluid to measure hydraulic power possess by the water at some height. The following relation is useful as in the following equation (1):

$$P_{\text{hyd}} = \rho g Q H, \tag{1}$$

where ρ is the water density, g is the gravitational acceleration, Q represents the volumatic water flow rate, and H is head available for water. So, the mechanical brake power can also be calculated by a given relation as in the following equation (2):

$$P_{\text{mech}} = \frac{2\pi N T_{\text{screw}}}{60}, \tag{2}$$

where N is the rotational speed of the turbine rotor, T_{screw} is the torque generated by the rotor. In addition, hydraulic performance can be found in the given relation as in the following equation (3):

$$\eta = \frac{P_{\text{mech}}}{P_{\text{hyd}}} = \frac{2\pi N T_{\text{screw}}}{\rho g Q H 60}. \tag{3}$$

The screw's performance is mostly determined by the various losses in the screw. There are several losses, including viscous friction of the water on the turbine surface, leakage flow via the space between the blade and the trough, and overflow of water through the central cylinder available in the water when struck on the turbine surface. Furthermore, the total flow Q, which can be expressed as in the following equation (4):

$$Q = Q_{\text{w}} + Q_{\text{l}} + Q_{\text{over}}, \tag{4}$$

where Q_{l} is the flow rate of water from leakage, Q_{over} is the overflow volume flow rate and Q_{w} is the working flow rate which can be contributed for power generation. The working volume flow rate can be calculated based on the relation given in the following equation (5):

$$Q_{\text{w}} = \frac{V_{\text{b}} N n}{60}, \tag{5}$$

where V_{b} is the trapped amount of water between two successive blades in the turbine unit. The values of C_{P}, C_{T} and power output were calculated as expressed in Equations (6), (7), and (8), respectively.

$$C_{\text{P}} = \frac{P_{\text{mech}}}{\frac{1}{2}\rho A V^3}, \tag{6}$$

$$C_{\text{T}} = \frac{T}{\frac{1}{2}\rho A V^2 R}, \tag{7}$$

$$P_{\text{mech}} = T \times \omega, \tag{8}$$

where C_{p} and C_{T} represent the power coefficient and torque coefficient. Equally, both are the performance parameters which are used to evaluate the performance of turbine, where ρ is the water density, V is the flow velocity, A is the surface area of the turbine runner, and R is the radius of the turbine runner. According to the current literature, the Betz criterion has a maximum allowable value of power coefficient of 16/27. TSR is a dimensionless parameter that describes the rotational speed of the turbine blades in proportion to the velocity of the fluid and propels the turbine blades. TSR is an important parameter which helps to determine turbine

performance. It indicates how rapidly the turbine blade tips are moving in relation to the speed of the water. After the modification, TSR helps to optimize the turbine performance at different flow conditions. The mathematical relation of TSR is given in the following equation (9):

$$TSR = \frac{\omega R}{V}, \tag{9}$$

where R is the radius of the turbine blade, ω is the angular velocity of the turbine blades, and V is the flow velocity of the water.

3 | MATERIALS AND METHODS

Figure 1 demonstrates the research scheme of the current study. There are three different phases developed to carry out research work. In the first phase, a conceptual design of AST unit and found optimized design parameters using CFD approach. In the second phase, a prototyping and experimental study was conducted based on an optimized design of the AST unit. The findings revealed from CFD simulations and experimental data were compared to validate the results.

3.1 | AST fundamentals

The AST consists of one or more helical blades with inner and outer diameters of (D_i and D_o) and a cylindrical shaft with length of L. The blades are typically welded to the cylindrical shaft and may be inclined at an angle to the axis. The geometrical specifications of the AST blade are presented. The assumptions were established on the C_P values determined for aligned and inclined setups and provided by Zitti et al.[7] So, more studies and experimental model testing are needed to properly examine the potential use of this type of turbine in hydrokinetic applications. A number of parameters defining the AST geometry are included along with the literature-reported values for each, given in Table 1.

3.2 | AST blade selection

The selection of turbine blades is most important to obtain maximum power and improve turbine performance. In this work, the optimization of the geometric parameters of the AST blade was carried out using the CFD approach. The independent parameters range for the AST blade is listed in Table 2. Solidworks was used to create a 3D CAD model of the AST blade as shown in Figure 2.

3.3 | Flow analysis

The hydraulic load and velocity distribution on the AST blade surfaces are computed using CFD modeling of AST. The parts that follow provide a quick overview of CFD modeling.

3.3.1 | Physical model

The initial stage in CFD simulation is the construction of a 3-D physical model as illustrated in Figure 3. With ANSYS Fluent Design Modeller, a computational domain is constructed and an AST blade is located within it. To create a finer mesh near the turbine blade, the domain was further separated into the rotary domain and turbine domain. Figure 4 displays the 2-D view of computational domain.

After creating the computational domain in ANSYS Fluent design modeler, it is necessary to generate appropriate meshing to attain accurate results.[2] In this study, the unstructured and tetrahedron meshing was used due to the complexity of the turbine blade. The total number of elements and nodes is 400,634 and 78,291, respectively. To maintain a fair balance between accuracy and computing costs of the solution, the mesh was improved on the AST's surface. Figure 5A,B demonstrates an illustration of the front and side view of meshing utilized in the numerical simulations.

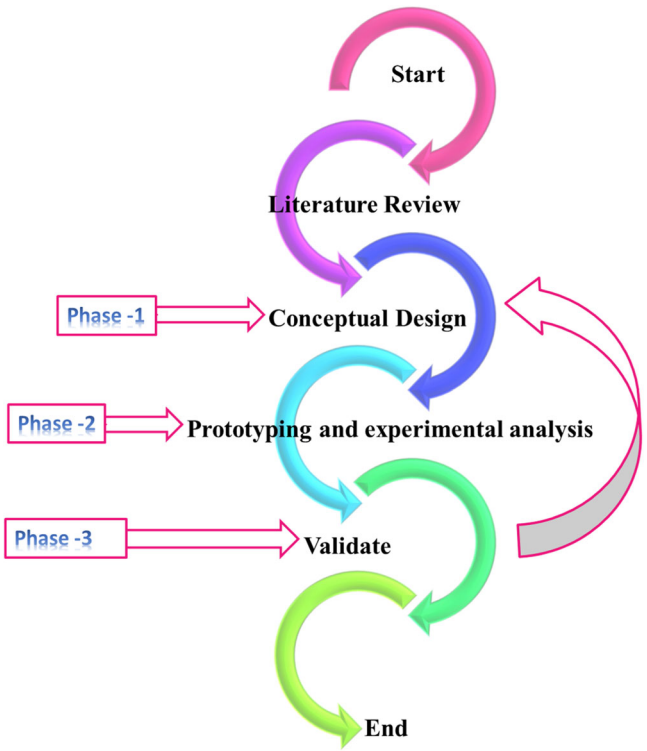

FIGURE 1 Research scheme of the study.

TABLE 1 Geometrical specifications and their values of AST blade from current literatures.

References	Application	Blade angle, α (°)	Inner diameter, D_i (m)	Outer diameter, D_o (m)	Length of blade, L (m)	Blade pitch, P (m)
Zitti et al.[7]	Hydrokinetic Turbine	70	0.04	0.1	0.320	0.160
Stergiopoulou et al.[32]	Hydrokinetic Turbine	90	0.1	0.2	1	0.2
Siswantara et al.[33]	Hydro Turbine	90	0.16	0.3	2.09	0.251
Dellinger et al.[6]	Hydro Turbine	90	0.106	0.192	0.4	0.192
Madrid et al.[34]	Hydro Turbine	90	0.696	1.3	5.739	2.241
Piper et al.[25]	Hydro Turbine	90	–	2	5	–
Kozyn and Lubitz et al.[26]	Hydro Turbine	90	0.1683	0.3252	1.229	0.033
Shahsavarifard et al.[35]	Hydrokinetic Turbine	60	0.21	1.06	2.87	0.637

TABLE 2 Independent parameters range for Archimedes screw turbine blade.

Design parameters	Values		
	Minimum value, −1	Medium value, 1	Maximum value, +1
Axl length, L, mm	700	850	1000
Blade pitch, P, mm	100	115	130
Blade width, b, mm	2	4	6

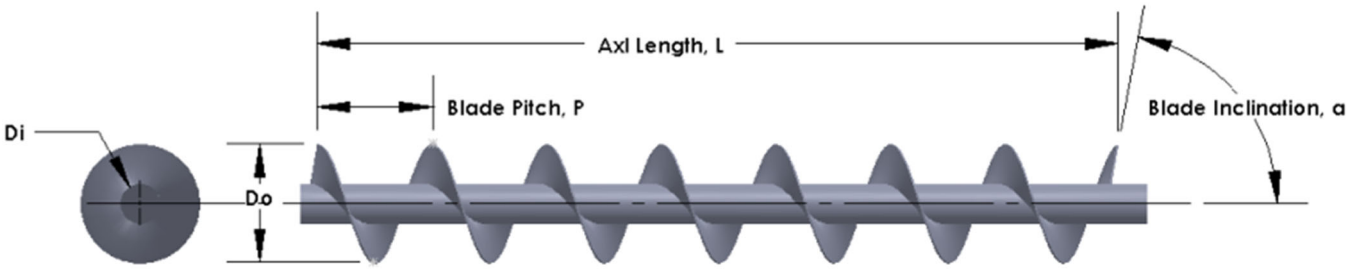

FIGURE 2 Geometrical specifications of Archimedes screw turbine blade.

3.3.2 | Governing equations and boundary conditions

The Reynolds number can be used to characterize the flowing field in the river near the turbine zone. The Reynolds number is expressed as follows in the following equation (10)[36]:

$$Re = \frac{\rho U_\infty D}{\mu}, \tag{10}$$

where Re denotes the Reynolds number, ρ is the fluid density, U_∞ is the free stream velocity, D is the diameter, and μ is dynamic viscosity. The numerical calculations were undertaken with Reynolds numbers of 14.33×106 for the outer diameter of the computational domain and 1.02×106 for the turbine runner tip diameter. The most useful turbulence model, the K-ω SST, is used for numerical simulation, which solves two independent transport equations to determine specific dissipation rate and turbulent kinetic energy. To run numerical simulations, the following assumptions are made: it has a three-dimensional stable state and incompressible flow as given in Equations (11) and (12).

Equation of conservation of mass:

$$\nabla \cdot \boldsymbol{u} = 0. \tag{11}$$

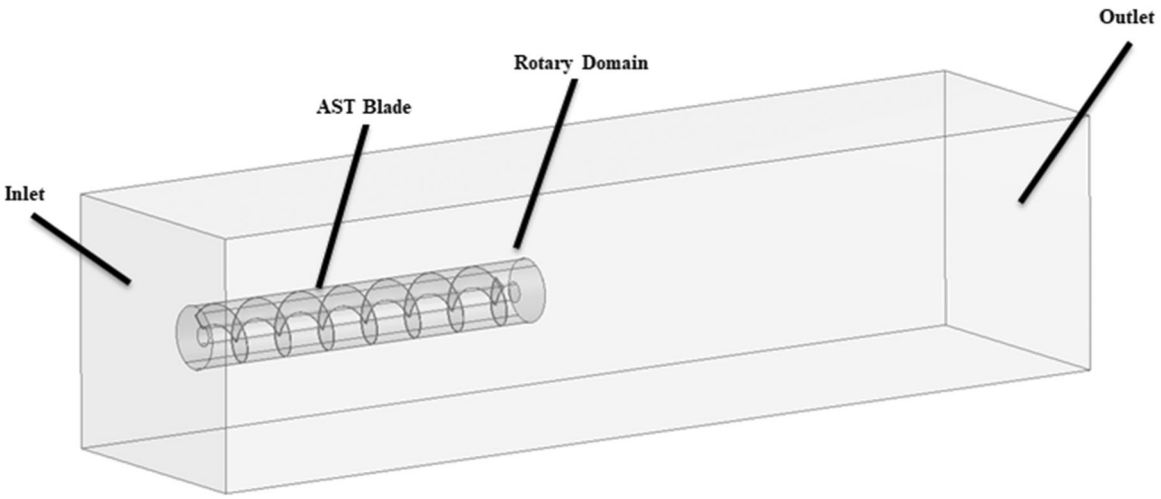

FIGURE 3 Three-Dimensional view of computational domain.

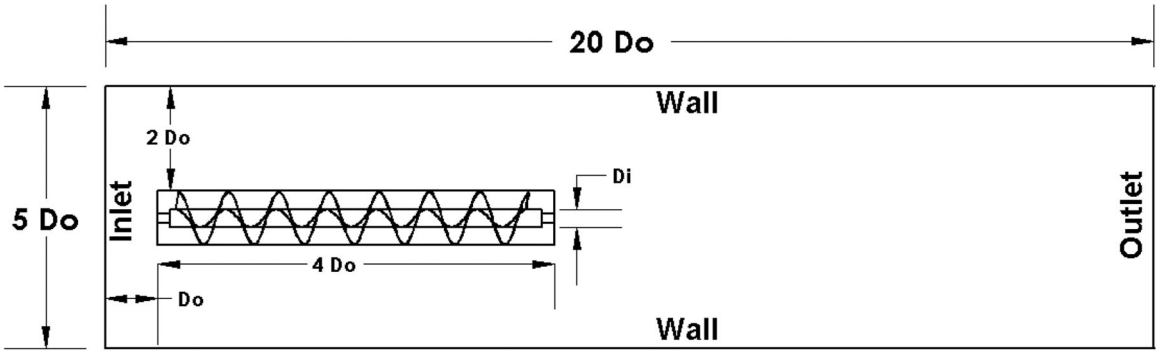

FIGURE 4 Specifications of computational domain.

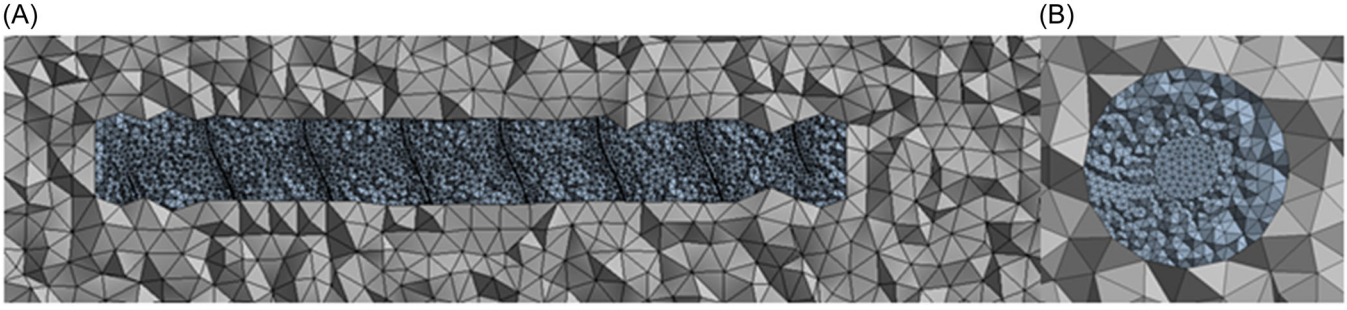

FIGURE 5 Mesh around the Archimedes screw turbine blade. (A) Front view and (B) side view.

Equation of conservation of momentum

$$\rho\left(\frac{\partial \boldsymbol{u}}{\partial t} + \boldsymbol{u}\cdot\nabla\boldsymbol{u}\right) = -\nabla p + \nabla\cdot\tau + S_{\mathrm{M}}, \tag{12}$$

where $\boldsymbol{u}$ is representing the velocity vector, ρ shows the density, t denotes the time, p shows the pressure, τ represents the stress tensor, S_{M} is showing momentum source. The equation of turbulence kinetic energy is as follows in Equations (13) and (14):

$$\frac{\partial k}{\partial t} + U_j\frac{\partial k}{\partial x_j} = \tau_{ij}\frac{\partial U_i}{\partial x_j} - \beta^* k\omega + \frac{\partial}{\partial x_j}\left[(\nu + \sigma_k \nu_T)\frac{\partial k}{\partial x_j}\right]. \tag{13}$$

Equation of specific dissipation rate

$$\frac{\partial \omega}{\partial t} + U_j \frac{\partial \omega}{\partial x_j} = \alpha S^2 - \beta \omega^2 + \frac{\partial}{\partial x_j}\left[(\nu + \sigma_\omega \nu_T)\frac{\partial \omega}{\partial x_j}\right] + 2(1 - F_1)\sigma_{\omega 2}\frac{1}{\omega}\frac{\partial k}{\partial x_j}\frac{\partial \omega}{\partial x_j}, \quad (14)$$

where k represents the turbulence kinetic energy, ω denotes the specific dissipation rate, α is showing the closure coefficient, S shows the mean rate-of-strain tensor and F_1 is showing the blending functions.

3.3.3 | Mesh independence

A suitable mesh density plays an important role to get accurate solution since the computational cost and precision of the solution is highly dependent on the number of elements. In this research work, mesh independence studies are carried out at various refinement levels up to a point where there is no major variation in the solutions. To comprehend the mesh independence study, the simulation process is repeated with various mesh refinement levels. The various mesh refinement levels are listed in Table 3. To evaluate the mesh independence, the hydraulic load computed from a CFD simulation on the AST blade is nominated to vary the with altered mesh refinement level. The effect of mesh sensitivity on altering hydraulic load with various mesh refinement levels is depicted in Figure 6. The main purpose of this mesh independence study is to deliver the sensitivity of the findings after simulation.

The selected mesh refinement level of 4 is used for CFD analysis. It has the number of elements of 400,634 and number of nodes of 78,291 with an average orthogonal quality, aspect ratio, and skewness of 0.85, 1.82, and 0.22, respectively. According to mesh independent study results, the refinement level 4 is considered the best mesh and within the acceptable range for CFD simulations to ensure the accuracy of hydraulic load estimation at appropriate computational cost. The comparison of mesh quality with current literature is also listed in Table 4. In addition,[37] performed a mesh independence test for CFD analysis in HSHKT, and 181,627 with average aspect ratio, skewness, and orthogonal quality of 1.96, 0.25, and 0.84 were nominated. It is explored whether or not the computational results agree with the experimental results. Therefore, the current computational results are within an acceptable range. Similarly,[2] conducted a grid independence test for CFD analysis of propeller turbine runners and selected 4,080,993 total numbers of elements having skewness, aspect ratio, and average orthogonal quality of 0.23, 1.79, and 0.82, respectively. Therefore, the presented mesh parameters are within acceptable range.

TABLE 3 Description of mesh study for computational fluid dynamic simulations.

Mesh refinement level	Number of element	Number of nodes	Hydraulic load (kPa)
1	72,510	22,540	2.3485
2	129,678	38,610	2.3098
3	199,624	58,020	2.2871
4	400,634	78,291	2.2912
5	492,142	96,632	2.2885
6	575,411	102,649	2.2895
7	615,152	150,656	2.2900

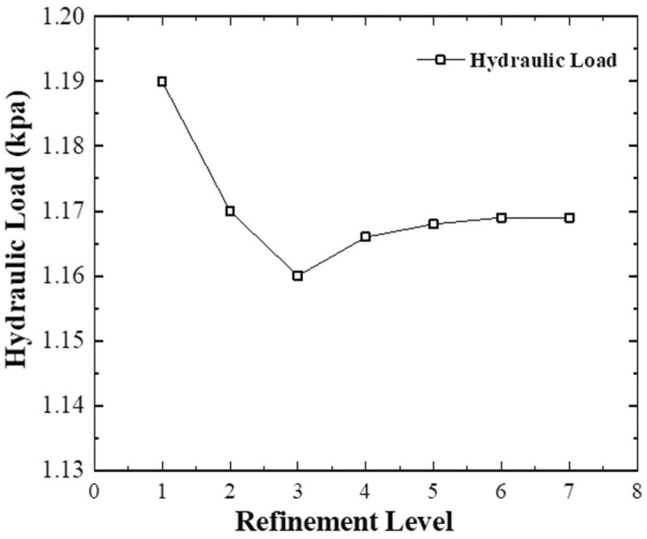

FIGURE 6 Variation of hydraulic load with different mesh refinement level.

TABLE 4 Comparison of mesh quality with current literature.

Mesh parameters/ paper	Average skewness	Average aspect ratio	Average orthogonal quality
Dinesh Kumar et al.[37]	0.25	1.96	0.84
Waqas et al.[2]	0.23	1.79	0.82
Present study	0.22	1.82	0.85

3.4 | Simulation procedure

CFD analyses of AST turbine blades are performed to compute the hydraulic load and examine the performance of turbine blades at different geometrical parameters. Initially, CFD analysis was accomplished to compute the hydraulic load on the surface. Then, the power output and other performance parameters are computed such as power coefficient and torque coefficient. Furthermore, for the diffusion term, the second order central differencing scheme was employed, and for the convection term, the second order upwind method was used. To achieve the pressure velocity iteration, the SIMPLEC algorithm was used. The overall pressure on the inflow border is determined by the water head. The static pressure is specified at the output boundary. The boundary condition of non-slip is used. In the case of a rotating wall, the rotational speed is also supplied. To accomplish solution convergence within a suitable limit, the residuals in the solution iteration are adjusted to 3–6 for solution convergence. The iterative approach is used to solve algebraic equations. The answer in the current investigation converges within the acceptable limit after 500 iterations. The flowchart of the methodology is shown in Figure 7.

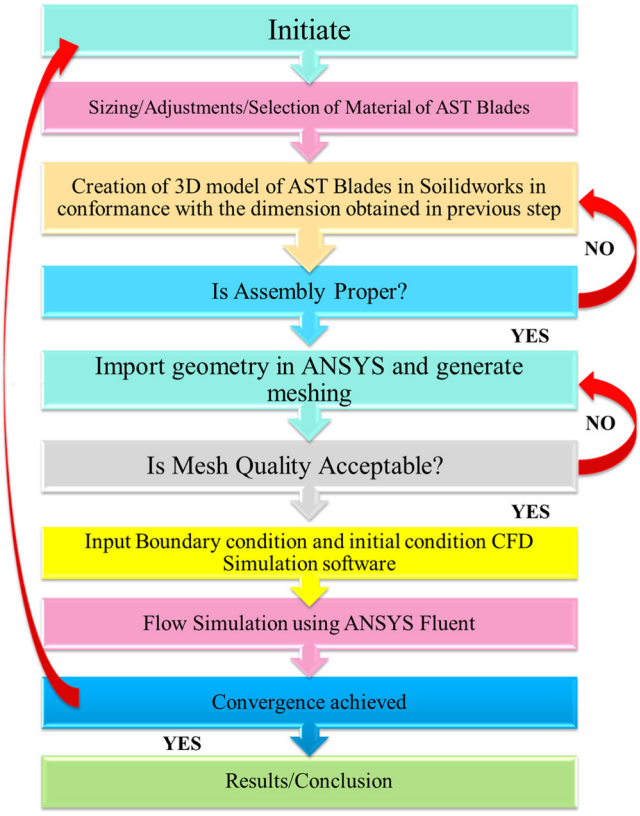

FIGURE 7 Numerical methodology flowchart. AST, Archimedes screw turbine; CFD, computational fluid dynamic.

4 | EXPERIMENTAL APPROACH

The experimental data was obtained from the low head AST unit which was set at the open water flowing channel as shown in Figure 8. The experimental system contained different components such as AST blade, AST frame, dynamo generator, chain and sprocket system, inlet, and discharge section. The experimental setup is placed within the open water flowing channel and makes it flexible at a specific water head for experimentation. The flowing water is directly come from the tube well which is flowing in the open channel and discharged from the discharge section. In a tube well discharge, a plate is placed to open the tube well discharge hole with different proportions such as 10%, 20%, 40%, 60%, 80%, and 100% and then determine the flow velocity accordingly. There are two universal bearings attached to the upper and lower sides of the AST turbine shaft which supports the AST screw shaft. In addition, a curve sheet and supporting frame which allow the water to move downstream from upper reservoir to lower reservoir. The 2 mm gap was set between the curve plate and AST blades which allow the AST unit to extract maximum kinetic energy from the flowing water. Table 5 represents the dimensions of the AST unit and other details in this study. Moreover, a dynamo generator with adjustable frequency drive was attached directly to the upper side of the AST unit. A load cell was devoted mechanically to the arm and an adjacent fixed point to the testing system frame. Because the load cell was the only method of preventing the gear motor from freely turning, the tension force measured by the load cell multiplied by the moment arm equalled the shaft torque generated by the screw and gear motor combination. The rotation speed of the screw was determined by passing a rare earth magnet affixed to the top of the screw's inner cylinder through a fixed magnetic switch multiple times. Water levels and flow in the system were changed for each performance measurement and then the system was given time to reach equilibrium. Over a 1-min average period, torque, rotation speed, water depths, and total flow rate through the system were all measured. In all testing scenarios, the water level in the open water flowing channel was left to change as needed to supply the requisite flow velocities into the screw.

5 | RESULTS AND DISCUSSION

Following the steps in Figure 7, the impact of various parameters such as blade width, blade pitch, and rotation angles on the performance of AST were investigated at different flow velocities.

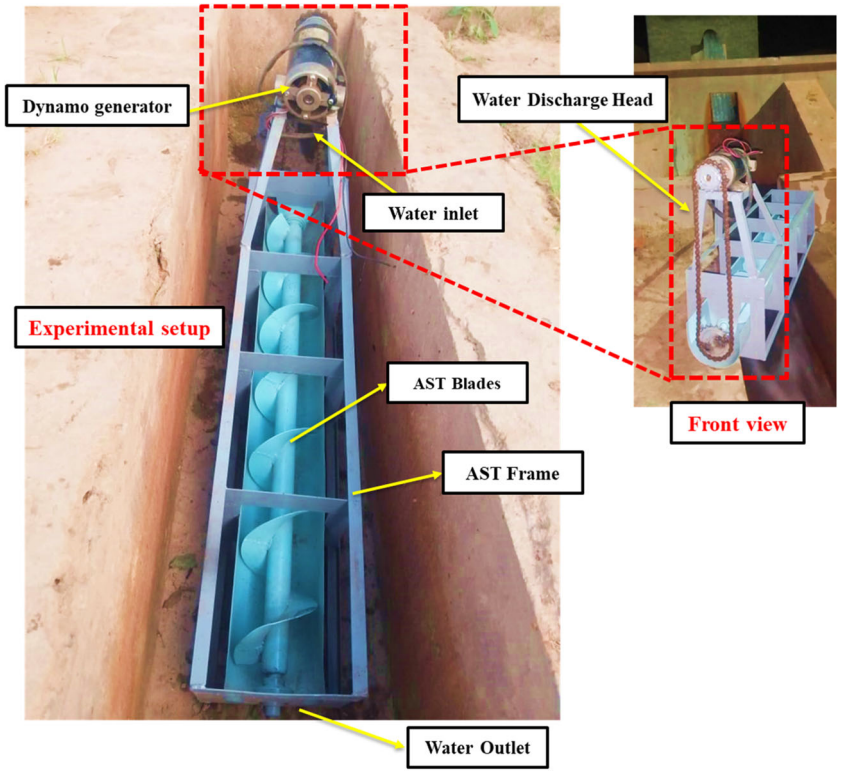

FIGURE 8 Experimental setup of low head Archimedes screw turbine power generation system.

TABLE 5 Technical specifications of turbine parameters and their values.

Parameters	Values
Blade slope, β	10°, 15°, 20°
Outer blade diameter, D_o	120 mm
Inner blade diameter, D_i	40 mm
Blade pitch, p	100, 115, 130 mm
Number of blade screws, N	1
Gap thickness, G_t	2 mm
Blade screw length, L	700, 850, 1000 mm
Materials	Mild steel
Elevation, H	1 m
Flow rate of pump, Q	10–80 LPM
Ambient temperature, T	25°C
Humidity, RH	55%
Water flow velocity, U	1–3.5 m/s

5.1 | Research findings and numerical validation

The experimental investigation of AST was conducted at different flow velocities such as 1, 1.5, 2, 2.5, 3, and 3.5 m/s. The revolutions per minute (rpm) generated by the experimental setup was measured using a digital tachometer. It was found from the experimental investigation that the flow and inclination angles greatly impacted by the rpm generated and the performance of the AST. Figure 9 represents the variation of power coefficient and torque with different flow velocities. It is evident from obtained results that by increasing the water flow rate would increase the system's kinetic energy. Hence, this will increase the rpm produced by the AST shaft. It was also examined from experiments that the rpm generated by AST decreases with the increasing of inclination angle except for 15° which shows maximum rpm. The results are consistent with those of Muller et al. and Dellinger et al., whose investigations also disclosed a tendency for efficiency to decrease with increasing turbine pitch angle.[16] However, it was further found, other parameters such as blade width, blade pitch and blade rotational angles are also important for design consideration. Findings from experimental investigation that the maximum turbine power coefficient of 0.51 and maximum torque of 2.8 Nm is achieved at blade width of 2 mm, blade pitch 130 mm and blade rotational angle 60° with water flow velocity of 2 m/s. The summary of optimized parameters is listed in Table 6.

The main aim of this paper is to examine the impact of blade pitch, blade width and blade rotational angle with different flow velocities. In addition, the influence of blade inclination angles were also evaluated at different flow velocities in the experimentation process.

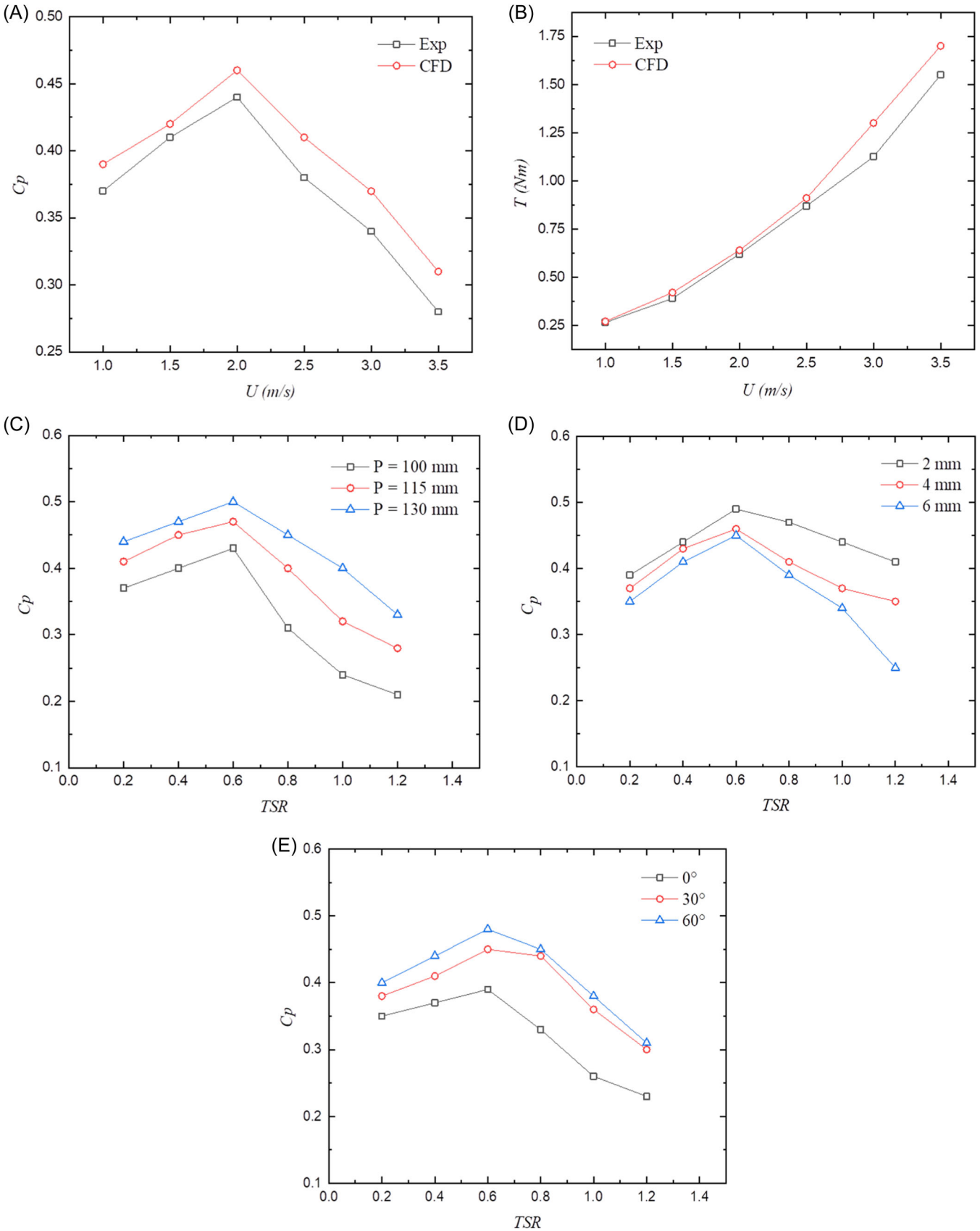

FIGURE 9 Comparison of experimental and computational fluid dynamic simulations results. (A) Power coefficient versus flow velocities, (B) tangential force versus flow velocities, (C) power coefficient versus tip speed ratio (TSR) for blade width, (D) power coefficient versus TSR for blade width, (E) power coefficient versus TSR for rotational angle.

TABLE 6 Summary of optimized design parameters and its values.

Parameters	Optimum values
Slope, β	15°
Outer diameter, D_o	120 mm
Inner diameter, D_i	40 mm
Pitch, p	130 mm
Number of screws, N	1
Gap thickness, G_t	2 mm
Rotation of turbine blade	160 rpm
Power coefficient, C_p	0.51

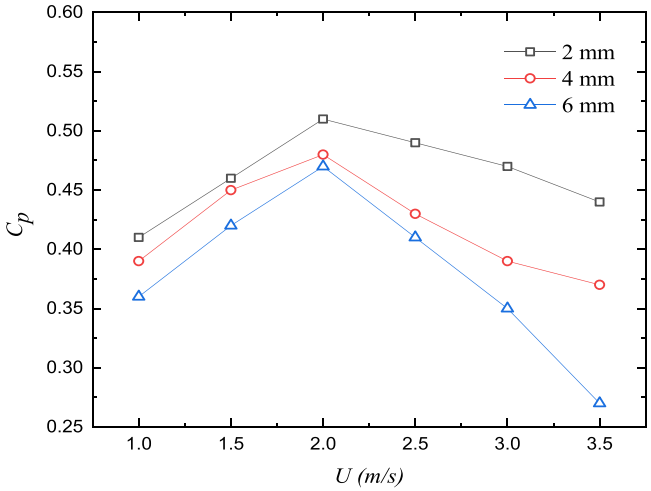

FIGURE 10 Variation of power coefficients with different flow velocities at different blade widths.

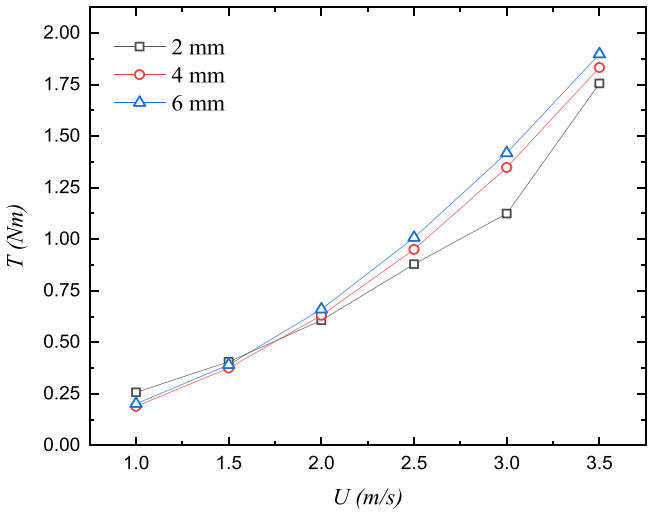

FIGURE 11 Variation of power torque with different flow velocities at different blade widths.

The outcomes obtained from CFD simulations were validated with experimental outcomes to ensure the data provided by the simulations was consistent. Precisely, the values of power coefficient and torque were compared to experimental outcomes for different flow velocities. Figure 9 represents the comparison of experimental and CFD simulations outcomes with different flow velocities. It can be seen from the computed results that the CFD simulation results is validated with experimental results with less than 5% error. Figure 9A shows the relationship between pressure coefficient and flow velocity. The trends show that when the pressure coefficient is sufficient, then the flow velocity is normal. Therefore, the correlation between simulation and experiment has coincided which validates the results. Likewise, Figure 9B shows the trends where on the maximum tangential force and the velocity of the water has an equal quantitative effect. Moreover, the relationship between power coefficient and TSR is shown in Figure 9C–E. This specific link pertains to the discussion of the influence of various specific parameters such as flow velocities, applied pressure, and rotation angle. The simulation results are in good correlation with the experiment results due to the sufficient tangential force using specific boundary conditions.

5.2 | Impact of blade width

CFD analyses of three different AST blades such as 2, 4, and 6 mm were performed at different flow velocities. The predicted performance curves of AST are shown in Figures 10 and 11 according to CFD simulations outcomes. According to computed results, power coefficient increases up to 2 m/s flow velocity and then decreases. The main reason behind this higher value is due to increment of rotational torque due to increasing water flow velocity. When the water flow velocity increases, the rotational torque of turbine blade is lowered down after a specific flow speed. The other main reason behind this variable graphical trend decrement is due to the filling of blade surface and the turbine blade rpm to decrease. Moreover, it has been revealed that the power coefficient rises as blade width falls. The blade width of 2 mm in Figure 10 produces the best results in terms of power coefficient. The similar behavior was also observed in some of the previous research articles such as Yang et al.[14] and Waqas and Ahmad.[2] The maximum and minimum values of power coefficient of 0.51 and 0.47 were observed as blade width of 2 and 6 mm, respectively. It was also found, with increasing flow velocity, the hydraulic load produces

more torque. It follows that to increase the performance of a hydraulic turbine, the blade width should be as narrow as is practical while maintaining a sufficient level of strength. Similarly, it was also examined from Figure 11 that maximum torque was generated for blade width of 6 mm and minimum torque was examined for blade width of 2 mm. The main reason behind this incremental value of torque for 6 mm blade width is due to the larger inertial force generated in 6 mm blade width case.

ANSYS fluent was used to perform the AST CFD analysis. The pressure distribution on the turbine runner surfaces reduces as the flow velocity decreases due to hydraulic load varies depending on operating conditions as shown in Figure 12. At a free stream velocity of 3.5 and 1.0 m/s, the highest pressure acting on the runner surface is 7.451 kPa and the minimum is −17.90 kPa. The pressure distribution on the turbine surfaces is irregular. As a result, the maximum pressure is recorded at the input and the smallest pressure is observed at the outflow of the runner. The pressure difference between the high and low pressure sides grows as the flow velocity of the water increases.

Moreover, flow velocity streamlines were also analyzed as shown in Figure 13. It can be seen that maximum flow velocity was observed at the edges of the turbine blade and minimum flow velocity was near the central rotating shaft. The vertexes can be observed around the helical shape of the blades. It can also be observed that maximum vertexes were observed at outlet of the turbine blades. Thus minimum flow velocity can be seen at outlet of the turbine blades.

5.3 | Impact of blade pitch

The impact of blade pitch is also an important parameter which strongly impacts on the performance of turbine. In this study, the impact of blade pitches on the performance of AST at different flow velocities. For this purpose, experimental and numerical simulations were performed. CFD analyses of three different blade pitches such as 100, 115, and 130 mm were performed at different flow velocities such as 1, 1.5, 2, 2.5, 3, and 3.5 m/s. Figures 14 and 15 represent the expected performance curves of AST according to CFD simulation outcomes. These figures show that power coefficient decreases with flow velocity. Moreover, it has been examined that the power coefficient rises as blade pitch increases. The blade width of 130 mm produces the best results in terms of power coefficient as shown in Figure 14. A few researchers examined the same research behavior and introduced the impact of blade pitch such as Bouvant et al.[11] and Shahverdi et al.[38] The maximum and minimum values of power coefficients of 0.51 and 0.44 were observed as blade pitch of 130 and 100 mm, respectively. It was also examined how the hydraulic load produces more torque as the flow velocity increases. Furthermore, the variation of torque generated at different flow velocities were also represented in Figure 15. It can be observed that the value of torque increased with water flow velocities. The more water flow

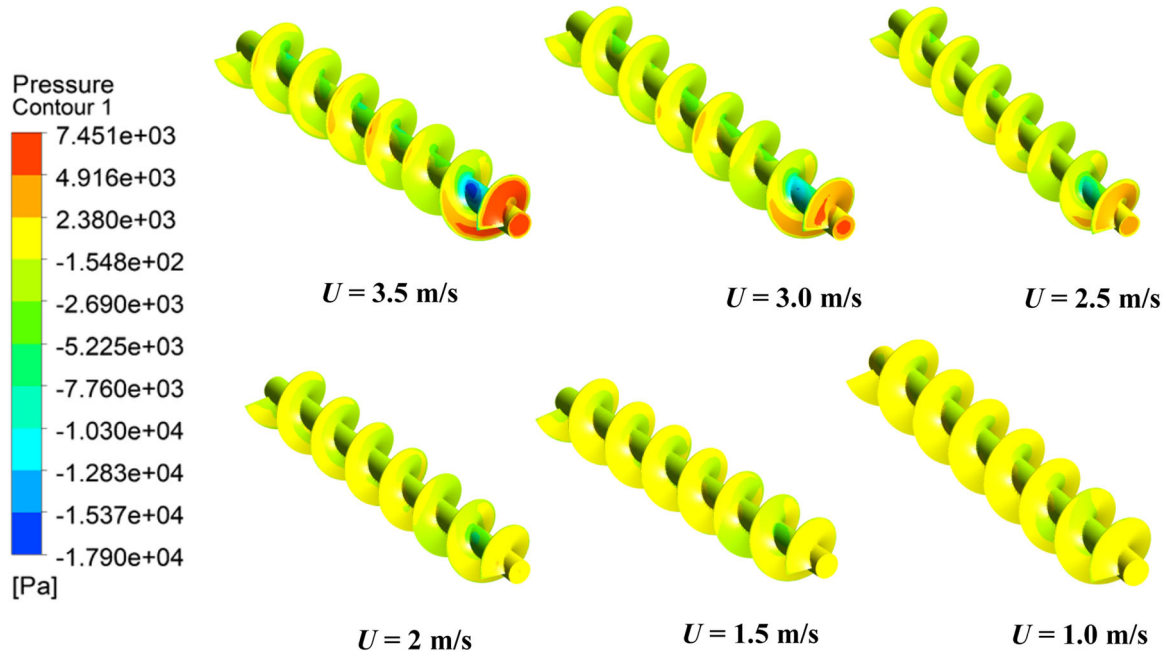

FIGURE 12 Pressure distribution on runner blade surfaces for blade width of 2 mm.

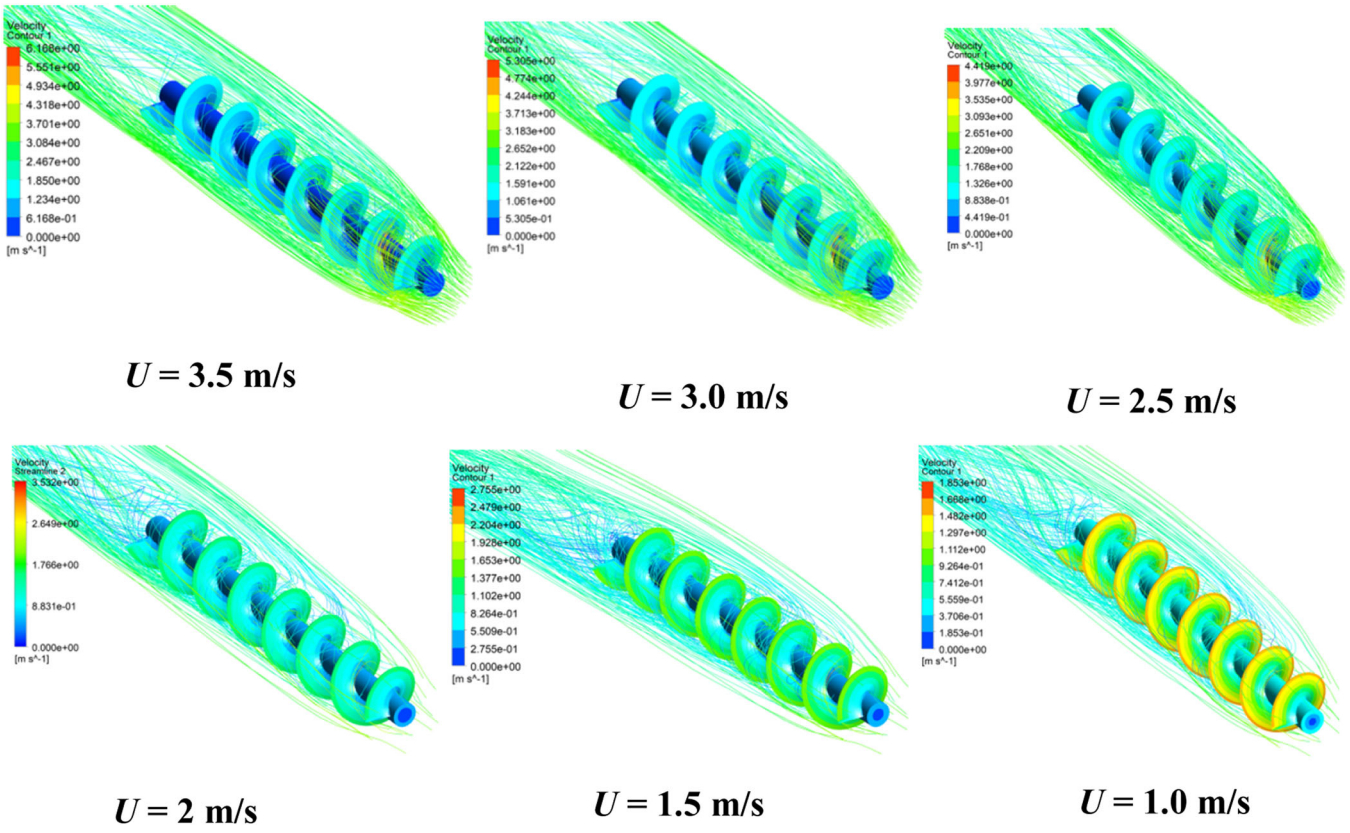

FIGURE 13 Flow velocity streamlines along the turbine blades for blade width of 2 mm.

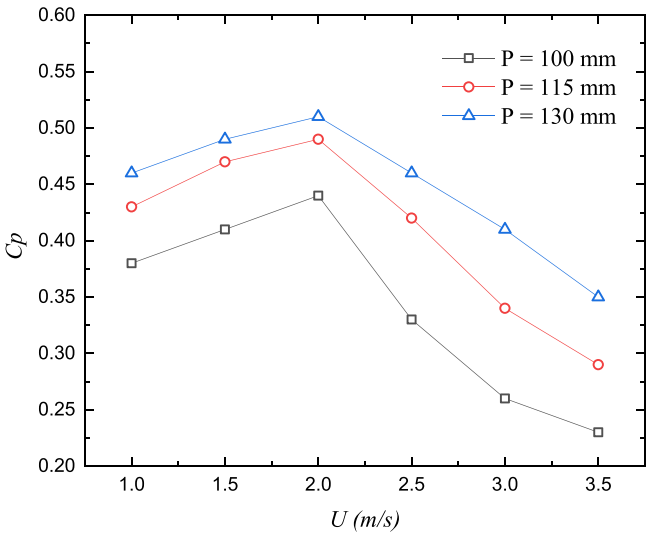

FIGURE 14 Variation of power coefficients with different flow velocities at different blade pitches.

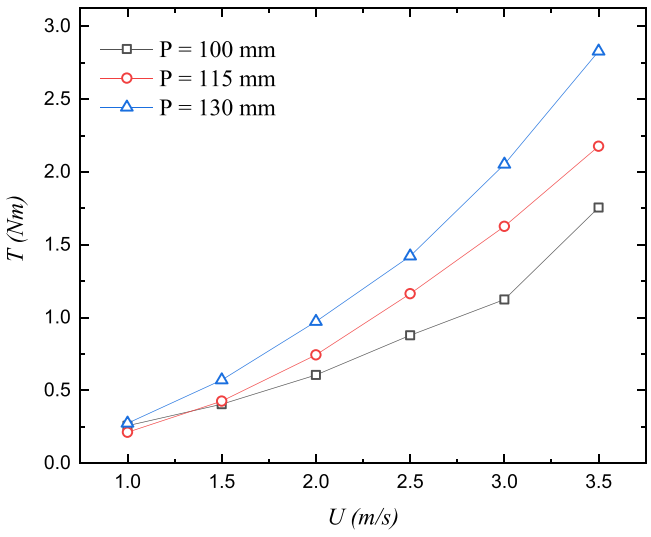

FIGURE 15 Variation of torque with different flow velocities at different blade pitches.

the torque increases, which may increase the power out at the turbine shaft which ultimately enhances the power output. It can be also examined that maximum torque was observed at a blade pitch of 130 mm and minimum was at 100 mm. The main reason behind this increment in torque value is that the more the distance between the one of blades to other adjacent blades, the more water entrapped the blades and generates more power. The maximum water energy can be converted into useful mechanical work by increasing the blade pitch.

Similarly, pressure distribution on the blade surfaces was investigated at various flow velocities. The pressure distribution on the turbine blade surfaces reduces as the flow velocity decreases, as seen in Figure 16. Maximum pressure was also noticed in the inlet section of the blade due to higher hydraulic load at the inlet of the turbine blade. At a free stream velocity of 3.5 and 1.0 m/s, the highest pressure acting on the runner surface is 7.263 kPa and the minimum is −17.61 kPa. The pressure distribution on the turbine surfaces is irregular. As a result, the greatest pressure is recognized at the runner's inlet and the minimum pressure is perceived at the runner's outflow.

In addition, flow streamlines over the turbine blades were also observed at different flow velocities, it can be examined that maximum flow velocities can be observed at outer side of the turbine blades and minimum near the central shaft of the turbine. The streamlines were also examined along the turbine blades. It can be seen from Figure 17 that maximum streamlines are shown in helical shape of the turbine and some streamlines are shown at outer side of the turbine blades. This is because of the gap between the turbine blades and the outer body of the turbine unit. This may lose some hydraulic energy which can be reduced by decreasing the gap between turbine blades and outer body.

5.4 | Impact of blade rotational angle

Rotational angles of turbine blades also greatly impacted the performance of turbines. In this study, CFD analyses of AST were conducted at three different rotational angles such as 0°, 30°, and 60° with different flow velocities. The performance curves of AST according to CFD simulations outcomes are represented in Figure 18. It is evident from Figure 18 that the maximum power coefficient was observed at 60° blade rotation. The reason behind this increment at 60° is due to maximum contact area exposed to water inlet. The maximum contact area exposed to water inlet recovers maximum hydraulic energy from the water inlet. Therefore, maximum power coefficient is achieved as compared to other blade rotational angles. In addition, it can also be seen that power coefficient increases till flow velocity of 2 m/s and then decreases. A similar phenomenon was observed and explained in previous studies.[20] Maximum value of power coefficient of 0.49 was observed at a flow velocity of 2 m/s and 60° blade rotation angle. Similarly, a minimum power coefficient of 0.41 was examined at a blade rotation angle of 0°. In addition, variations of torque with different flow velocities and blade rotation angles were represented in Figure 19. It can be seen from the investigations that torque is increased with the flow velocity and maximum torque was observed at 60° blade rotation angle. The maximum and minimum values of torque of 1.7 and 1.58 Nm were computed at blade rotation angle of 60° and 0°, respectively.

In this study, CFD analysis of the AST was carried out using ANSYS FLUENT. It is obvious from Figure 20 that when the flow velocity drops, the pressure distribution on the turbine runner surfaces also decreases. Since the hydraulic load depends on different operating conditions.

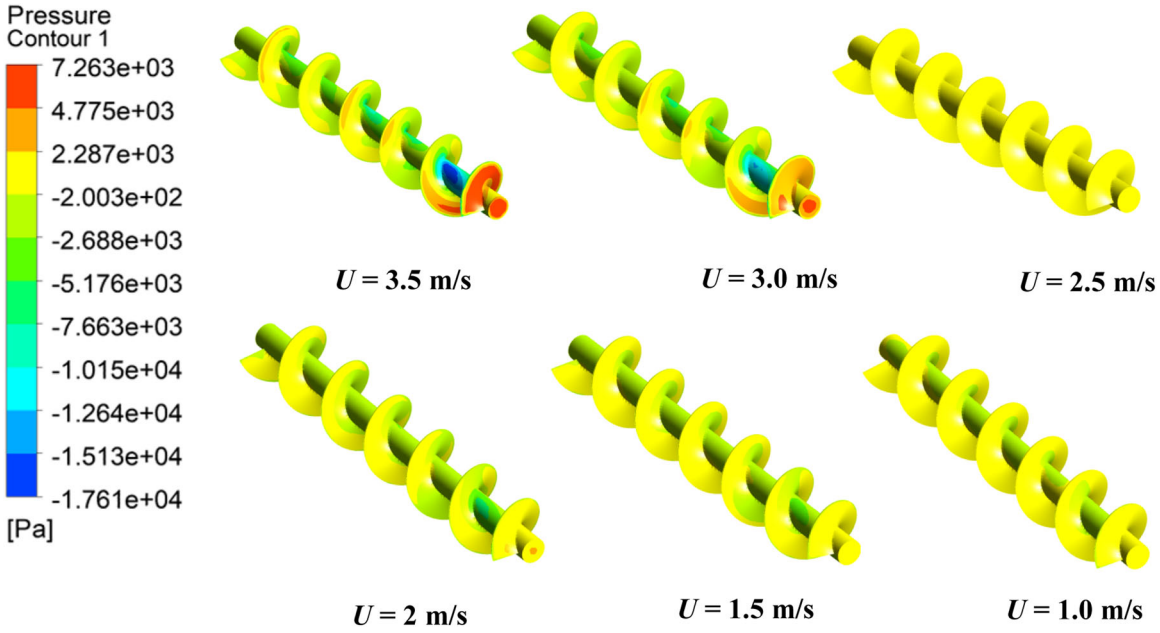

FIGURE 16 Pressure distribution on runner blade surfaces for blade pitched of 130 mm.

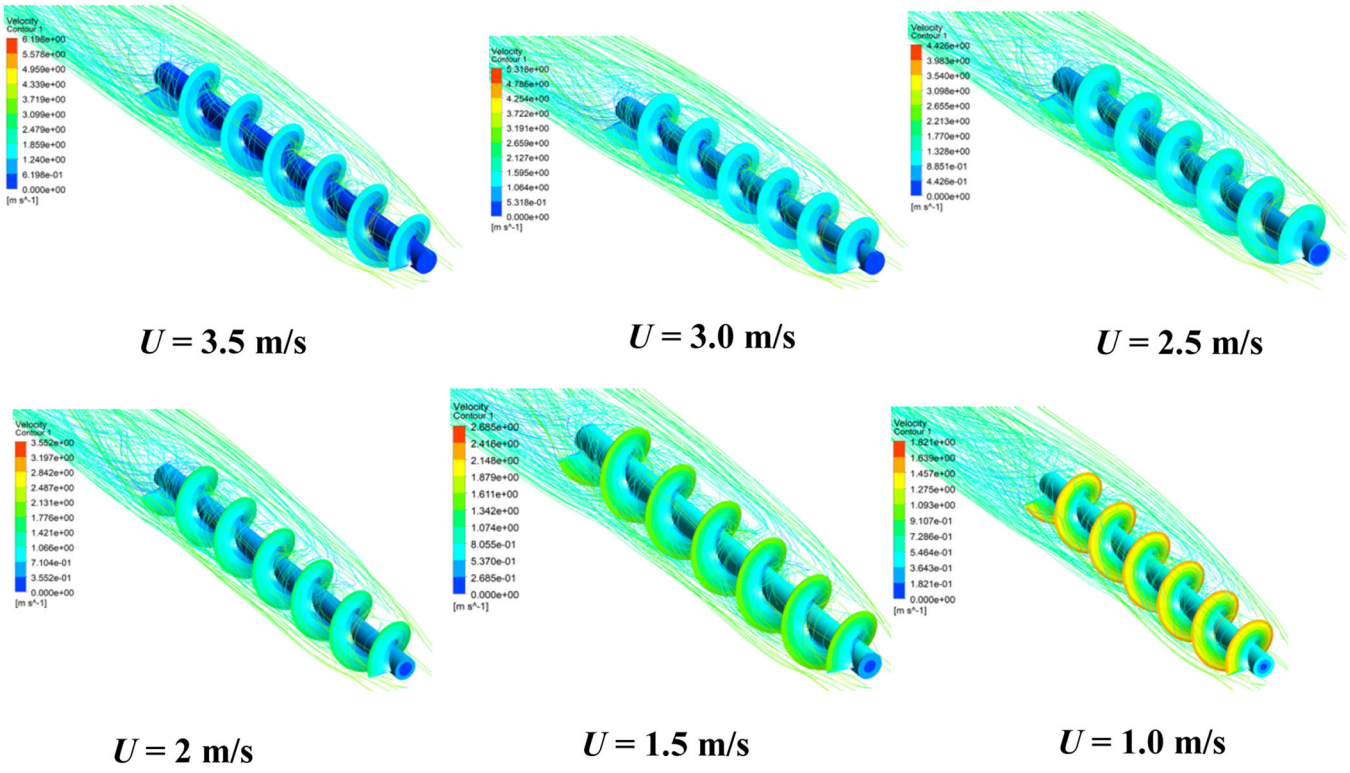

FIGURE 17 Flow velocity streamlines along the on turbine blade for blade pitched of 130 mm.

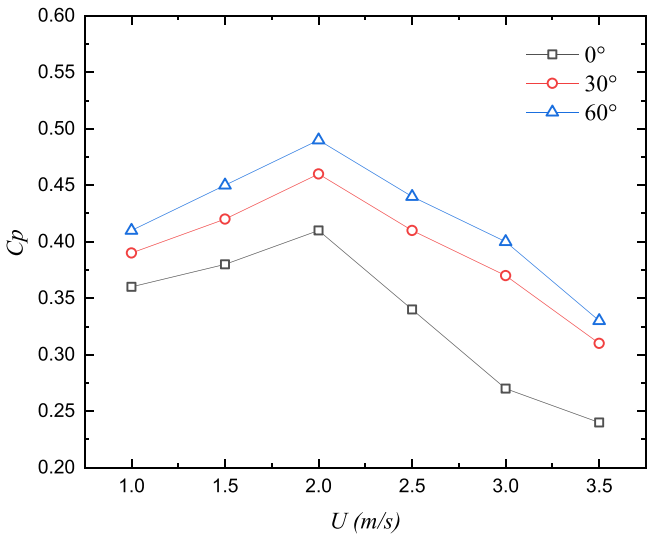

FIGURE 18 Variation of power coefficients with different flow velocities at different blade rotational angles.

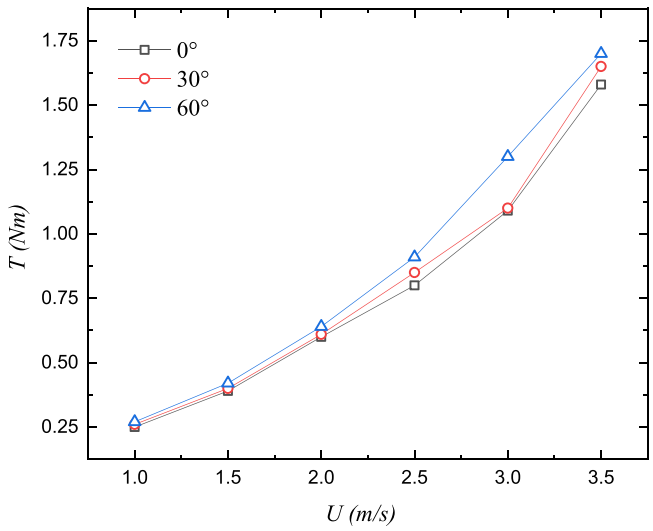

FIGURE 19 Variation of torque with different flow velocities at different blade rotational angles.

At free stream velocities of 3.5 and 1.0 m/s, respectively, it is noted that the highest pressure acting on the runner surface is 8.297 kPa and the minimum is −14.04 kPa. The pressure distribution is not homogeneous throughout the turbine surfaces. Therefore, it is also shown that the runner's intake and outflow have the highest and lowest pressures, respectively. As the water's flow velocity rises, the gap between the sides of high and low pressure widens.

In addition, Figure 21 represented a velocity distribution and flow stream over turbine blades. It can be seen from the Figure that maximum velocity was examined at the outer surface of the turbine blade and minimum velocity can be shown at the central area of the turbine

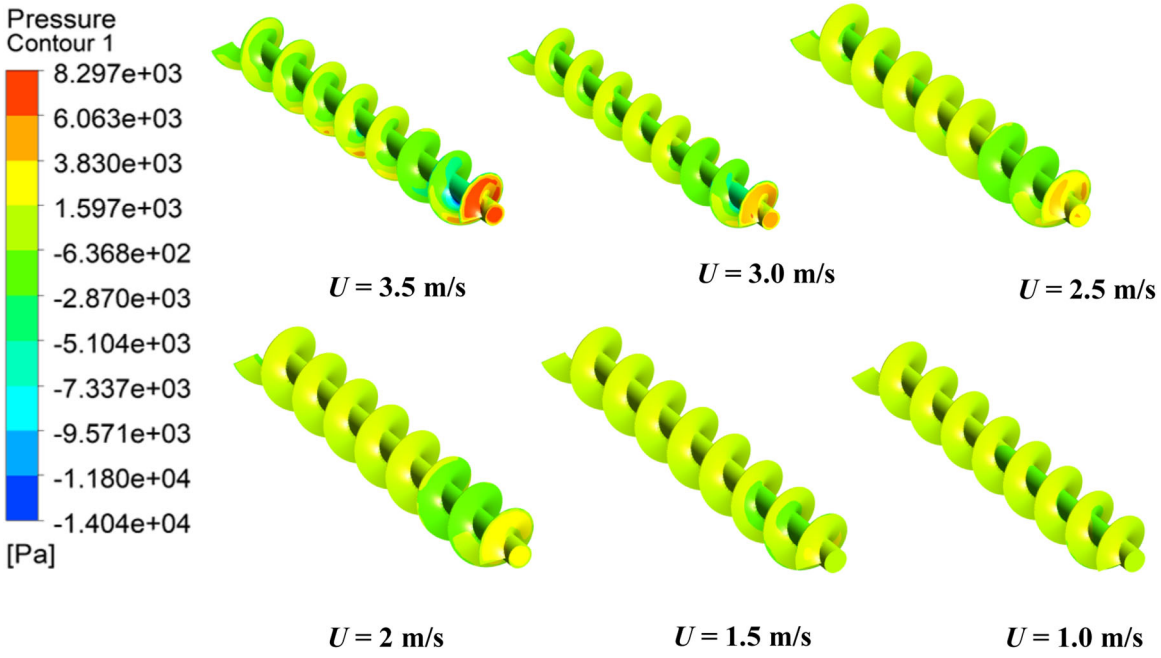

FIGURE 20 Pressure distribution on turbine blade surfaces for blade rotational angle of 60°.

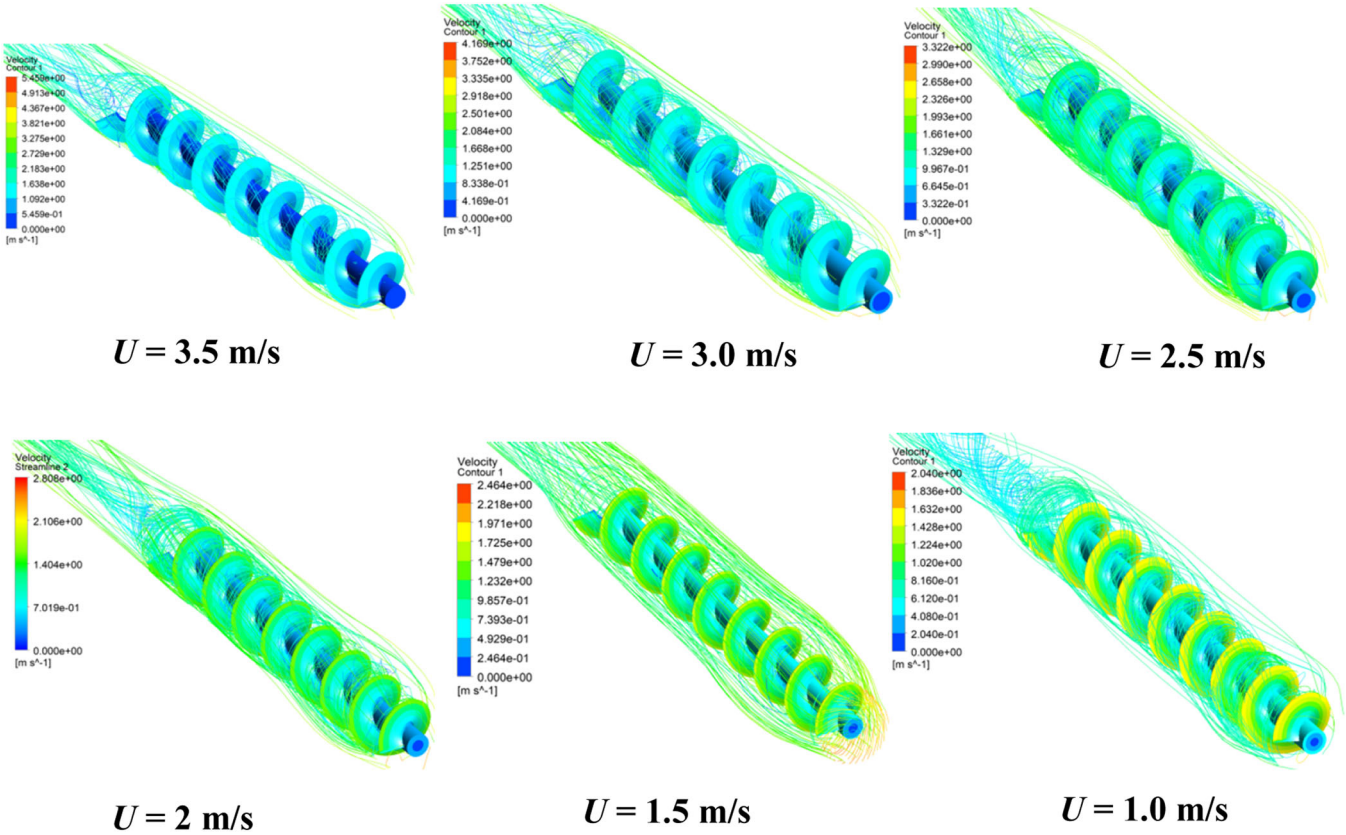

FIGURE 21 Flow velocity streamlines along the turbine blade for a blade rotational angle of 60°.

blades. Moreover, vertexes are generated at outer section of turbine blades due to helical rotation of the turbine blades. It is also evident that maximum vertexes were generated for flow velocity of 1 m/s and minimum vertexes were observed for flow velocity of 3.5 m/s. The reason behind this increment in vertexes for flow velocity of 1 m/s is due to maximum contact of water with helical shape of the blade which may result in maximum vertexes.

6 | CONCLUSIONS

The paper investigated the performance of an AST for open water flow channel application. The simulations were performed for three different design parameters such as blade width, blade pitch and blade rotational angles. The comprehensive conclusions drawn from this study are given below;

1. The performance of AST is greatly affected by the design parameters such as blade width, blade pitch, and blade rotation angles.[11,20,38] The performance of AST was examined in terms of power coefficient (C_p) and torque (T). The maximum power coefficient was achieved at design parameters of blade width 2 mm, blade pitch 130 mm, and blade rotation angle of 60°.
2. Similarly, the flow characteristics of the AST blade are determined using the CFD approach. The flow characteristics over the turbine blade were evaluated in terms of pressure distribution, velocity distribution and flow streams. It was investigated that maximum pressure was observed on the frontal side of the blades and minimum pressure on the back side of the turbine blades.[2] The maximum value of pressure was recorded at flow velocity of 3.5 m/s and minimum value of pressure was examined at flow velocity of 1 m/s. In addition, maximum flow vertexes were generated at the exit of the blades.
3. The maximum value of power coefficient of 0.51 was recorded at flow velocity of 2.5 m/s and for design configuration of 2 mm blade width, 130 mm of blade pitch and 60° of blade rotation angles.
4. Moreover, experimental study has also been carried out for the consistency of CFD simulation outcomes. The experimental study was conducted at an open channel river flow location. The optimal design parameters were used for experimentation and validated with CFD data in the same design configurations.
5. It was investigated that the experimental outcomes are in good agreement with CFD simulations results with less than 5% error. The optimized design parameters such as blade width, blade pitch and blade rotation angles are worthy of consideration for design of AST unit.
6. Based on the current research, it is concluded that additional work for the AST under other distinct conditions, such as alternative blade materials, is required. The current research also investigates the requirement to consider fluid-structural analysis, fatigue analysis, and vibrational analysis under various frictional losses of AST for structural performance assessment.

NOMENCLATURE

LATIN

C	coefficient
D	diameter (m)
L	axle length (m)
Re	Reynolds number
U	velocity (m/s)
Cp	power coefficient
P_{hyd}	hydraulic power
P_{mech}	mechanical power
TSR	tip speed ratio

GREEK SYMBOL

P	blade pitch
μ	dynamic viscosity (Pa s)
ρ	density (kg/m^3)
α	blade inclination angle

SUBSCRIPTS

a	absolute
b	blades
H	hydraulic
I	inlet
O	outlet
t	blade width

AUTHOR CONTRIBUTIONS

Conceptualization: Zeshan Abbas. *Data curation*: Zeshan Abbas, Muhammad Waqas, Saad Saleem Khan, and Rabia Khatoon. *Formal analysis*: Zeshan Abbas, Stephen Larkin, and Zhao Lun. *Funding acquisition*: Stephen Larkin. *Investigation*: Muhammad Waqas, Rabia Khatoon, and Priyanka Priyanka. *Methodology*: Zeshan Abbas. *Project administration*: Saad Saleem Khan and Stephen Larkin. *Resources*: Saad Saleem Khan. *Software*: Muhammad Waqas. *Supervision*: Saad Saleem Khan. *Validation*: Zeshan Abbas, Muhammad Waqas, and Zhao Lun. *Visualization*: Zeshan Abbas. *Writing—original draft*: Zeshan Abbas and Muhammad Waqas. *Writing—review and editing*: Rabia Khatoon, Stephen Larkin, and Zhao Lun. All authors have read and agreed to the published version of the manuscript.

ACKNOWLEDGMENTS

This research is funded by Africa New Energies Limited, UK and National Natural Science Foundation of China (No. 12104324), Scientific Research Startup Fund for Shenzhen High-Caliber Personnel of SZPT (No. 6022310046K), Postdoctoral Startup Fund of

Shenzhen Polytechnic University (Nos. 6021330001K and 6022331008K).

CONFLICT OF INTEREST STATEMENT

The authors declare no conflict of interest.

DATA AVAILABILITY STATEMENT

The authors declare that the data presented in this study are available within the article.

ORCID

Zeshan Abbas https://orcid.org/0000-0001-6850-3374
Lun Zhao http://orcid.org/0000-0001-8293-9094

REFERENCES

1. Shahverdi K. Modeling for prediction of design parameters for micro-hydro Archimedean screw turbines. *Sustain Energy Technol Assess*. 2021;47(September):101554. doi:10.1016/j.seta.2021.101554
2. Waqas M, Ahmad N. Computation of stress distribution in hydraulic horizontal propeller turbine runner based on fluid—structure interaction analysis. *Arab J Sci Eng*. 2020;45:9325-9337. doi:10.1007/s13369-020-04727-9
3. Havn TB, Sæther SA, Thorstad EB, et al. Downstream migration of Atlantic salmon smolts past a low head hydropower station equippped with Archimedes screw and Francis turbines. *Ecol Eng*. 2017;105:262-275. doi:10.1016/j.ecoleng.2017.04.043
4. Yuce MI, Muratoglu A. Hydrokinetic energy conversion systems: a technology status review. *Renew Sustain Energy Rev*. 2015;43:72-82. doi:10.1016/j.rser.2014.10.037
5. Shahverdi K, Loni R, Maestre JM, Najafi G. CFD numerical simulation of Archimedes screw turbine with power output analysis. *Ocean Eng*. 2021;231(June 2020):108718. doi:10.1016/j.oceaneng.2021.108718
6. Dellinger G, Garambois PA, Dellinger N, et al. Computational fluid dynamics modeling for the design of Archimedes screw generator. *Renew Energy*. 2018;118:847-857. doi:10.1016/j.renene.2017.10.093
7. Zitti G, Fattore F, Brunori A, Brunori B, Brocchini M. Efficiency evaluation of a ductless Archimedes turbine: laboratory experiments and numerical simulations. *Renew Energy*. 2020;146:867-879. doi:10.1016/j.renene.2019.06.174
8. Shahverdi K, Loni R, Ghobadian B, et al. Energy harvesting using solar ORC system and Archimedes screw turbine (AST) combination with different refrigerant working fluids. *Energy Convers Manage*. 2019;187(October 2018):205-220. doi:10.1016/j.enconman.2019.01.057
9. Monatrakul W, Suntivarakorn R. Effect of blade angle on turbine efficiency of a spiral horizontal axis hydro turbine. *Energy Procedia*. 2017;138:811-816. doi:10.1016/j.egypro.2017.10.075
10. Li J, Zhang Y, Liu K, Xian H, Yu JX. Numerical simulation of hydraulic force on the impeller of reversible pump turbines in generating mode *. *J Hydrodyn*. 2017;29(4):603-609. doi:10.1016/S1001-6058(16)60773-4
11. Bouvant M, Betancour J, Velásquez L, Rubio-Clemente A, Chica E. Design optimization of an Archimedes screw turbine for hydrokinetic applications using the response surface methodology. *Renew Energy*. 2021;172:941-954. doi:10.1016/j.renene.2021.03.076
12. Shahverdi K, Loni R, Ghobadian B, Gohari S, Marofi S, Bellos E. Numerical optimization study of Archimedes screw turbine (AST): a case study. *Renew Energy*. 2020;145:2130-2143. doi:10.1016/j.renene.2019.07.124
13. Riglin J, Schleicher W. Computational fluid dynamics and structural finite element analysis of a micro hydro turbine. ASME International Mechanical Engineering Congress and Exposition. 2013;5:1-8(February 2013). doi:10.1115/IMECE2013-65474
14. Yang SS, Wang C, Chen K, Yuan X. Research on blade thickness influencing pump as turbine. *Adv Mech Eng*. 2014;6:190530. doi:10.1155/2014/190530
15. Dedić-Jandrek H, Nižetić S. Small scale archimedes hydro power plant test station: design and experimental investigation. *J Clean Prod*. 2019;231:756-771. doi:10.1016/j.jclepro.2019.05.234
16. Dellinger G, Simmons S, Lubitz WD, Garambois PA, Dellinger N. Effect of slope and number of blades on Archimedes screw generator power output. *Renew Energy*. 2019;136:896-908. doi:10.1016/j.renene.2019.01.060
17. Daskiran C, Attiya B, Riglin J, Oztekin A. Large eddy simulations of ventilated micro hydrokinetic turbine at design and off-design operating conditions. *Ocean Eng*. 2018;169(Sep-September):1-18. doi:10.1016/j.oceaneng.2018.09.008
18. Riglin J, Schleicher WC, Oztekin A. Numerical analysis of a shrouded micro-hydrokinetic turbine unit. *J Hydraul Res*. 2015;53(4):525-531. doi:10.1080/00221686.2015.1032375
19. Teran LA, Larrahondo FJ, Rodríguez SA. Performance improvement of a 500-kW Francis turbine based on CFD. *Renew Energy*. 2016;96:977-992. doi:10.1016/j.renene.2016.05.044
20. Erinofiardi E, Nuramal A, Bismantolo P, et al. Experimental study of screw turbine performance based on different angle of inclination. *Energy Procedia*. 2017;110(December 2016):8-13. doi:10.1016/j.egypro.2017.03.094
21. Kozyn A, Lubitz WD. A power loss model for Archimedes screw generators. *Renew Energy*. 2017;108:260-273. doi:10.1016/j.renene.2017.02.062
22. Lee MD, Lee PS. Modelling the energy extraction from low-velocity stream water by small scale Archimedes screw turbine. *J King Saud Univ Eng Sci*. 2023;35(xxxx):319-326. doi:10.1016/j.jksues.2021.04.006
23. Lisicki M, Lubitz W, Taylor GW. Optimal design and operation of Archimedes screw turbines using Bayesian optimization. *Appl Energy*. 2016;183:1404-1417. doi:10.1016/j.apenergy.2016.09.084
24. Liu H, Geng Z, Gu Y, et al. A regional integrated energy system with a coal-fired CHP plant, screw turbine and solar thermal utilization: scenarios for China. *Energy Convers Manag*. 2020;212(April):112812. doi:10.1016/j.enconman.2020.112812
25. Piper AT, Rosewarne PJ, Wright RM, Kemp PS. The impact of an Archimedes screw hydropower turbine on fish migration in

a lowland river. *Ecol Eng*. 2018;118(August 2017):31-42. doi:10.1016/j.ecoleng.2018.04.009

26. Rohmer J, Knittel D, Sturtzer G, Flieller D, Renaud J. Modeling and experimental results of an Archimedes screw turbine. *Renew Energy*. 2016;94:136-146. doi:10.1016/j.renene.2016.03.044
27. Siswantara AI, Budiarso W, Harmadi R, Gumelar MH, Adanta D. Investigation of the α angle's effect on the performance of an Archimedes turbine. *Energy Proc*. 2019;156:458-462. doi:10.1016/j.egypro.2018.11.084
28. Bohadan V. Assessment of pretreatments and enzymatic hydrolysis of wheat straw as a sugar source for bioprocess industry. *J. Energy*. 2010;3(5):427-446. doi:10.1018/j.engergy.2010.13.096
29. Khan A, Khattak A, Ulasyar A, Imran K, Munir MA. Investigation of Archimedean screw turbine for optimal power output by varying number of blades. *1st International Conference on Electrical, Communication, and Computer Engineering (ICECCE) 2019*. 2019. July:1-6. doi:10.1109/ICECCE47252.2019.8940654
30. Kashyap K, Thakur R, Kumar R, Kumar S. Feasibility analysis for conversion of existing traditional watermills in Western Himalayan region of India to micro-hydropower plants using a low head Archimedes screw turbine for rural electrification. *Int J Ambient Energy*. 2022;43(1):7463-7473. doi:10.1080/01430750.2022.2068056
31. Kumar Thakur N, Thakur R, Kashyap K, Goel B. Efficiency enhancement in Archimedes screw turbine by varying different input parameters—an experimental study. *Mater Today Proc*. 2022;52:1161-1167. doi:10.1016/j.matpr.2021.11.020
32. Erinofiardi, Agus N, Putra B, Abhijit D, Aliakbar A, Afdhal KM, Ahmad FS. Experimental study of screwturbine performance based on different angle of inclination. *Energy Procedia*. 2017;110(8):1-6. doi:10.1016/j.egypro.2017.03.094
33. Zeshan A, Muhammad W. Strategy on coal consumption and GHGs emission analysis based on the LEAP model: a case study. Energy sources, Part A: Recovery, Utilization and Environmental Effects. 2020; 1(00): 1-21. doi:10.1080/15567036.2020.1783392
34. Madrid ME, Toro JM, Ortega S. Hydrodynamic screws as an alternative for small hydropower generation in Colombia. *WIT Trans Ecol Environ*. 2015;195:15-23. doi:10.2495/ESUS150021
35. Shahsavarifard M, Birjandi AH, Bibeau EL, Sinclaire R. Performance characteristics of the Energy Cat 3EC42 hydrokinetic turbine. *MTS/IEEE Ocean. 2015—Genova Discov. Sustain. Ocean Energy a New World*. 2015:3-6. doi:10.1109/OCEANS-Genova.2015.7271420
36. Riglin J, Carter F, Oblas N, Schleicher WC, Daskiran C, Oztekin A. Experimental and numerical characterization of a full-scale portable hydrokinetic turbine prototype for river applications. *Renew Energy*. 2016;99:772-783. doi:10.1016/j.renene.2016.07.065
37. Kumar D, Sarkar S. Modeling of flow-induced stress on helical Savonius hydrokinetic turbine with the effect of augmentation technique at different operating conditions. *Renew Energy*. 2017;111:740-748. doi:10.1016/j.renene.2017.05.006
38. Shahverdi K, Najafi G, Mamat R, Ghazali MF, EI-Shafy AS, Mousa M. Introducing a design procedure for Archimedes screw turbine based on optimization algorithm. *Energy Sustain Dev*. 2023;72(December 2022):162-172. doi:10.1016/j.esd.2022.12.004

How to cite this article: Abbas Z, Waqas M, Khan SS, Khatoon R, Larkin S, Zhao L. Numerical and experimental investigation of an Archimedes screw turbine for open channel water flow application. *Energy Sci Eng*. 2023;1-20. doi:10.1002/ese3.1649